Characteristics of the aerodynamic interference between two high-rise buildings of different height and identical square cross-section

Huang Dongmei[*1,2], Zhu Xue[1], He Shiqing[1], He Xuhui[1,2] and He Hua[1]

[1]*School of Civil Engineering, Central South University, Changsha 410075, China*
[2]*High-speed Railway Construction Technology National Engineering Laboratory, Changsha 410075, China*

Abstract. In this work, wind tunnel tests of pressure measurements are carried out to assess the global aerodynamic interference factors, the local wind pressure interference factors, and the local lift spectra of an square high-rise building interfered by an identical cross-sections but lower height building arranged in various relative positions. The results show that, when the interfering building is located in an area of oblique upstream, the RMS of the along-wind, across-wind, and torsional aerodynamic forces on the test building increase significantly, and when it is located to a side, the mean across-wind and torsional aerodynamic forces increase; In addition, when the interfering building is located upstream or staggered upstream, the mean wind pressures on the sheltered windward side turn form positive to negative and with a maximum absolute value of up to 1.75 times, and the fluctuating wind pressures on the sheltered windward side and leading edge of the side increase significantly with decreasing spacing ratio (up to a maximum of 3.5 times). When it is located to a side, the mean and fluctuating wind pressures on the leading edge of inner side are significantly increased. The three-dimensional flow around a slightly-shorter disturbing building has a great effect on the average and fluctuating wind pressures on the windward or cross-wind faces. When the disturbing building is near to the test building, the vortex shedding peak in the lift spectra decreases and there are no obvious signs of periodicity, however, the energies of the high frequency components undergo an obvious increase.

Keywords: tall buildings; wind tunnel pressure measurements; global aerodynamics interference factor; local wind pressure interference factor; local lift spectra

1. Introduction

The various specifications and standards relating to wind engineering (e.g., GB 50009-2012 2012, ASCE 7-10 2010, NBCC 2010 2010, and so on) very seldom provide any effective guidance to the structural designer on the subject of aerodynamic interference. However, compared to single buildings, the wind load and wind-induced response on a disturbed building are very different because of the effect of mutual interference between buildings and the convection field-even to the

---

∗Corresponding author, E-mail: huangdongmei_tumu@163.com

extent that the interference would appear to have an amplification effect (Taniike 1992, Khanduri *et al*. 1998, Thepmongkorn *et al*. 2002, Xie and Gu 2004, Hui *et al*. 2013, Mara *et al*. 2014, Ke *et al*. 2015). Therefore, studying the increment in wind load resulting from aerodynamic interference has important ramifications both theoretically and practically and is of great value to the wind-resistant design of structures including glass curtain walls.

The relative positions of adjacent buildings are the most important parameters to consider in the study of wind interference effects (Blazik 2006, Zhao and Lam 2008, Lim and Bienkiewicz 2014, Mara *et al*. 2014). When the distance between buildings is small, the flow between them may be greatly changed. Whether an interfering building is located in the upstream, downstream, or to one side of the object building, will have a different effect on the surface wind pressure, aerodynamic coefficients, and vibrational response of the object building. It is usually assumed that the interference effect between two buildings gradually weakens as the distance between them increases. Essentially, the interference effect disappears when the separation exceeds a certain distance.

In addition to studies of the effect of interference on the wind-induced response of high-rise buildings (Thepmongkorn *et al*. 2002, Mara *et al*. 2014), researches have also been carried out on the interference effect on the wind loads acting on high-rise building groups mainly based on the overall aerodynamic forces (e.g. drag, lift, and torsion torque) and local pressures. The effect of interference on the power spectra of the tail flow and aerodynamic force has also been investigated (Huang and Gu 2005, Lam *et al*. 2008). The existing literature concerning wind-load interference effects in super-high-rise buildings has been mainly focused on interference effects in the total wind load (Sakamoto and Haniu 1988, English 1990, Xie and Gu 2004, Zhao and Lam 2008, Mara *et al*. 2014). Studying the interference effects of overall aerodynamic force resulting from different relative positions of the disturbing and disturbed buildings, allows a very intuitive approach to be made. One can find out which positions lead to more obvious interference effects on the average and fluctuating aerodynamic forces, and, in particular, which positions cause increased adverse interference and what exactly is the degree of interference involved. Thus, a reference for the engineer can be provided by which the overall static wind load on the building can be estimated and the corresponding interference amplification factors can be considered.

Although the overall aerodynamic force can be holistically, intuitively, and simply expressed, it cannot give a good explanation of the mechanisms responsible for the aerodynamic interference under various conditions. It also does not give further guidance to the design of glass curtain walls. Therefore, there is a small section of the literature that is focused on the disturbance effects of the local wind pressure on the surface of the building, or the flow field around it (Kim *et al*. 2011, Hui *et al*. 2012, Hui *et al*. 2013, Wang *et al*. 2014). In those studies, wind tunnel tests and particle image velocimetry (PIV) flow visualization experiments were used to investigate the interference characteristics of the local wind loads on the building surface and the velocity of the surrounding flow field. The results indicate that the local wind pressure on the building surface is increased significantly when the two buildings are close together. The flow velocity between the two buildings is also significantly increased.

Investigations of the power spectrum of the aerodynamic force resulting from the disturbance of a building structure are aimed at the *whole* aerodynamic force (Huang and Gu 2005, Lam *et al*. 2008). This work has shown that when the distance between the two buildings is small, the aerodynamic power spectrum undergoes great change. This is especially so in the across-wind and torsional spectra in which the vortex shedding peak becomes significantly reduced, and the high frequency turbulence energy increases. Studying the interference characteristics of aerodynamic

power spectra is useful when explaining the characteristics of the vibrational response to the disturbance and helps provide a deeper understanding of the change in the vortex shedding characteristics and turbulence signature of the building in the frequency domain.

Although some studies on the interference effects in two typical high-rise buildings have done so (Hui *et al*. 2013, Xie and Gu 2005, Mara *et al*. 2014), few studies have comprehensively investigated the interference characteristics, degree, and mechanisms relating to the global and local wind loads, and the aerodynamic spectra. In addition, the interference effects on an object building caused by a downstream disturbing building are seldomly considered.

In this work, we use rigid models of square-sectioned high-rise buildings as research objects to carry out pressure measurements in a wind tunnel. The aim is to study in details the interference effects in the wind load acting on a square building when an identical cross-sectioned, and slightly shorter, disturbing square building is located at different relative positions surrounding the disturbed building. First, the interference factors of integral overall mean and fluctuating aerodynamic forces at different relative positions are analysis in detail. This allows us to directly and conveniently analyze in which positions the interference factors are amplified or attenuated. It also provides a reference for the preliminary design of the structures employed. The interference effects of the local wind pressure on the disturbed building were further studied using some typical configurations : that is, tandem, side-by-side, and staggered for various different spacing ratios (the minimum center–center distance is 1.5*D*, where *D* is the width of the buildings). Individually defined interference factors for the local mean and fluctuating wind pressure coefficients were adopted to intuitively analyze the degree of increase or decrease in the mean and fluctuating wind pressures acting on different surfaces and at different heights of the disturbed building resulting from the disturbing building located in different relative locations and spacing ratios, The outcomes can provide a reference for the design of glass curtain walls and help explain the mechanism of the aerodynamic interference. Finally, for each of the three configurations (tandem, side-by-side, and staggered), fluctuating layer lift spectra for the disturbed building are analyzed and compared in detail for different spacing ratios. This helps us to understand the interference characteristics of the vortex shedding and the turbulence signatures of the disturbed building.

2. Wind tunnel tests

2.1 Wind field simulations

The experiments were carried out in the high-speed railway tunnel of the National Engineering Laboratory of High-speed Railway Construction Technology of the Central South University, China. The wind tunnel is a double test-section reflux type tunnel. It comprises of a low-speed test section which is $12 \, \text{m} \times 3.5 \, \text{m} \times 18 \, \text{m}$ (width $\times$ height $\times$ length) in size and uses wind speeds ranging from 2 to 18 m/s. The high-speed test section measures $3 \, \text{m} \times 3 \, \text{m} \times 15 \, \text{m}$ (width $\times$ height $\times$ length) and uses winds from 2 to 90 m/s. All the experiments reported in this paper were carried out in the high-speed section (see Fig. 1). According to the standards outlined in GB50009-2012 (2012), a category C flow field in the atmospheric boundary layer can be simulated in the wind tunnel using a passive simulation method.

For our tests, a geometrical scale of 1:350 was adopted. A reference point was further defined at a height of 1.2 m, and the reference test wind speed at the reference height was chosen as 14 m/s.

Fig. 2 shows the simulated along-wind mean speeds and turbulence intensity profiles, and the power spectrum of the along-wind fluctuating velocity (the latter at the reference height). The targeted theoretical values in the load codes are also shown. As can be seen from Fig. 2, the simulations are in good agreement with the theoretical values and so meet the requirements of the research.

2.2 Test model profile

The test model (i.e., the disturbed building) is a square-sectioned cylinder 163 mm × 163 mm × 1403 mm (width × width × height) in size (implying an aspect ratio of about 1:8.6). The disturbing model has the same cross-section but a height of 1200 mm, so the disturbing-model: disturbed-model height ratio is about 0.86. The relative layout of the two models (disturbing and disturbed) is shown in Fig. 3, in which the positions of disturbing model include upstream, downstream, and a side, and the minimum center–center distance is 1.5D (D is the common length of the sides of the models).

Fig. 1 Photograph of the wind tunnel used in the tests

(a) Mean wind profile   (b) Turbulence intensity profile   (c) Power spectrum of the fluctuations in the along-wind
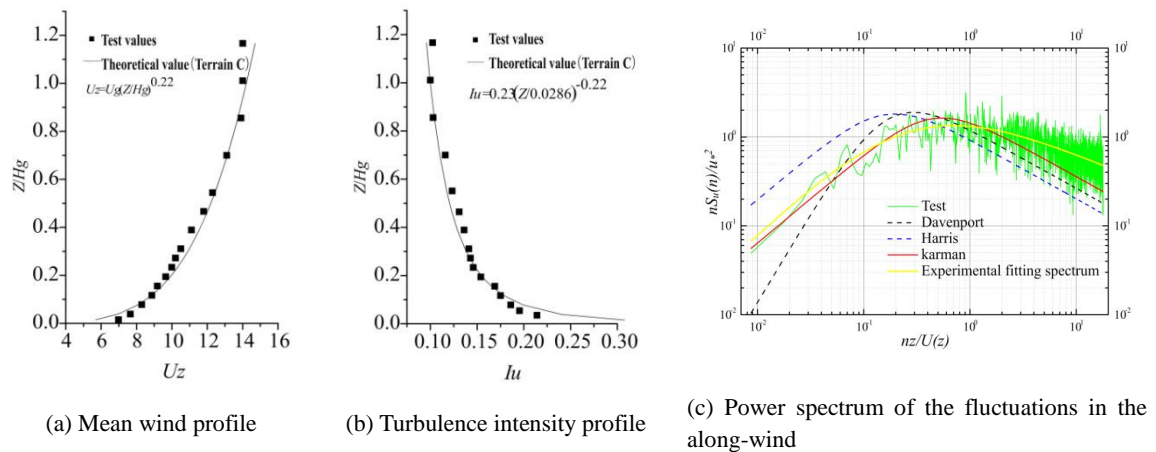
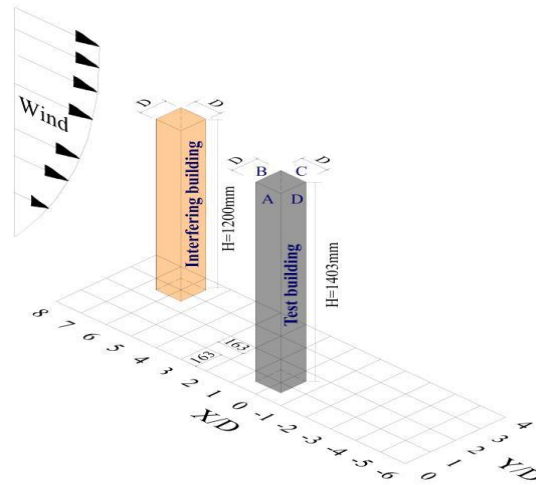Fig. 2 Simulated wind parameters for the category C terrain employed.

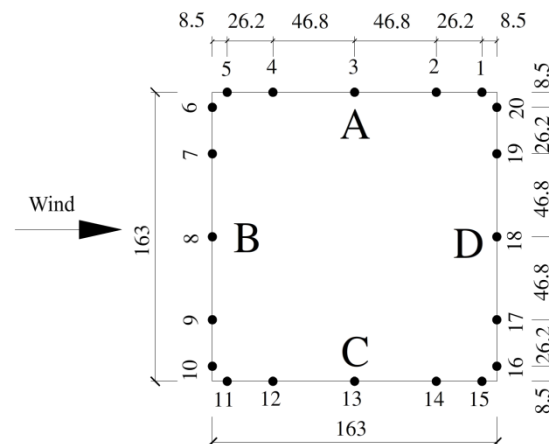Fig. 3 Arrangement of the interfering and disturbed models

Fig. 4 Arrangement of the measuring points

In this figure, X/D and Y/D correspond to the spacing ratios in along-wind (X) and across-wind (Y) directions, respectively. The disturbed building had measuring points along its height in 6 layers, corresponding to heights of 228, 603, 803, 1003, 1203, and 1328 mm, respectively. (Note that the 5th layer is slightly higher than the disturbing building, and the 6th layer is higher than the disturbing model by about $0.8D$). The 1st layer represents the lower part, the 2nd–4th layers the middle parts, and the 5th–6th layers the upper parts, so that the 6th layer corresponds to the top of the disturbing model.) The arrangement of the measuring points is consistent within each layer, as shown in Fig. 4. The measurement points on the surface of the model are connected with a pressure scanning valve via a PVC tube of 0.6 mm internal diameter and 20 cm length. The sampling frequency of the scanning valve is 625 Hz, and the number of samples in each channel is 20,000.

2.3 Definition of the interference factors

In this work, aerodynamic interference factors (AIFs) are defined in the following manner:

$$\mathrm{AIF} = \frac{C_{\mathrm{a\_int}}}{C_{\mathrm{a\_iso}}} \quad \text{or} \quad \frac{C'_{\mathrm{a\_int}}}{C'_{\mathrm{a\_iso}}} \tag{1}$$

where, C_{a} represents an aerodynamic coefficient (drag coefficient, lift coefficient, and torque coefficient) which are obtained by Integrating of local instantaneous pressures (Huang *et al.* 2015), and subscripts 'iso' and 'int refer to the test building in isolation and in the interference state, respectively. Unprimed quantities correspond to mean values and primed ones to root mean square (RMS) values of the overall quantities.

When a local analysis is performed, the interference factor (I_f) at the particular measuring point is defined in terms of wind pressure coefficients (C_{p}) as follows

$$I_f = \frac{C_{\mathrm{p\_int}}}{C_{\mathrm{p\_iso}}} \tag{2}$$

$$I'_f = \frac{C'_{\mathrm{p\_int}}}{C'_{\mathrm{p\_iso}}} \tag{3}$$

Here, the same subscript and priming conventions are used as for Eq. (1). Hence, I_f (I'_f) corresponds to the interference factor based on the local average (fluctuating) wind pressure coefficients and the ratios compare the disturbed building to the undisturbed state.

Eqs. (1)-(3) make it clear that the interference factors tend to 1.0 as the interference effects become negligible. Also, interference factors (including absolute valued ones) that are >1.0 imply a greater degree of disadvantageous interference. Similarly, values that are <1.0 (including absolute values) imply a greater degree of advantageous interference. A negative interference factor indicates that the aerodynamic force is reversed.

3. AIF analysis

Before doing an AIF analysis, wind tunnel tests need to be carried out according to the sketch shown in Fig. 3: the object test model is fixed at the location (0, 0), and the disturbing model is placed and moved in turn to each location considered (the minimum distance between the centers of the two models is 1.5D). The body-fixed axes of both the disturbing and disturbed models are in agreement with the wind axes, and all of the wind angles are fixed at 0°. In the contour maps that follow, the incoming flow is always shown coming from the right and moving to the left. In this paper, the positive along-wind direction corresponds to the negative X axial direction, and the positive across-wind direction corresponds to the negative Y axial direction. A positive torque value corresponds to the counter-clockwise direction.

In this section, several interference factors are discussed: the AIFs derived using the RMS values of the aerodynamic coefficients in the along-wind, across-wind, and torque directions; the AIFs derived from the along-wind mean aerodynamic coefficients; and those found from the mean measured aerodynamic coefficients in the cross-wind and torque directions (the aerodynamic

coefficients in the across-wind and torque directions are theoretically zero in the isolated state).

3.1 Along-wind AIFs

In the along-wind direction, the disturbance is mainly reflected by a decrease in the average wind speed (due to the effect of shielding) and a change in turbulence (caused by wake turbulence) which has a more complicated effect on the fluctuating wind load acting on the downstream building. A contour plot of the AIF values derived from the along-wind mean aerodynamic force for terrain C is shown in Fig. 5. It can be seen from the figure that: (1) When the disturbing model is located upstream, the AIF values are smaller than those for a single building. They also decrease as the distance ratio decreases (the minimum value is close to 0.2). This reflects an obvious shielding effect. In addition, the locations of the right upstream are just the valley of the contour of interference factor. (2) When the disturbing model is located downstream of the disturbed model, the AIF values change little. They are concentrated in the range 0.8 to 1.0 (a shallow valley in the contour is formed at $45°$) and indicate that there is little interference in these positions. (3) When the disturbing model is located to the side of the disturbed model, the AIF values decreases as the distance ratio decreases. If the distance ratio is larger than 2.0, the interference is negligible. The distribution of the AIFs derived from the RMS values of the along-wind aerodynamic force for terrain C is shown in Fig. 6. The figure tells us that: (1) When the disturbing model is located right upstream, the AIF values mostly lie in the range 0.5 to 1.0, which indicates that the fluctuating energy of the along-wind aerodynamic force is reduced. (2) When the disturbing model is located in an area oblique to the upstream by $5°$ to $30°$, the AIF value ranges from 1.0 to 1.3.
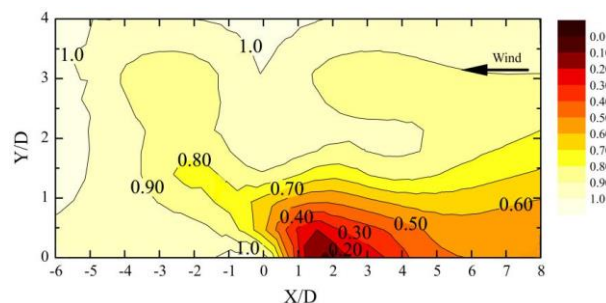

Fig. 5 AIF contour plot of the mean along-wind aerodynamic force for terrain C
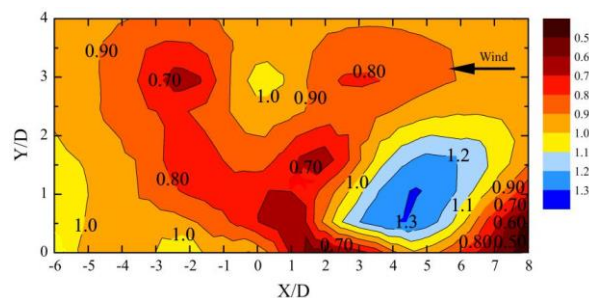

Fig. 6 AIF contour plot of the RMS along-wind aerodynamic force for terrain C

This is due to the effect of the shear flow from the disturbing model and incoming flow, which causes the fluctuating intensity of the along-wind aerodynamic force to increase in an obvious manner. The peak ridge line of the contour is at about 15° and the peak itself is approximately located at ($4.5D$, $1D$). (3) When the disturbing model is located to the side and downstream, the AIF values are mainly in the range 0.8 to 1.0, and there is a valley in the contours at about 45°.

3.2 Across-wind AIFs

The interference occurring in the cross-wind aerodynamic force basically arises from vortex shedding, which is generally more complex than the interference in the along-wind case. For a single building, the mean value of the cross-wind aerodynamic force is theoretically equal to zero as the windward side of the model is perpendicular to the incoming flow and the surfaces are symmetrical. Thus, an analysis of the distribution of the AIFs for the mean cross-wind aerodynamic force has little significance. Therefore, we only give here a contour map relating to the mean across-wind aerodynamic force coefficients (Fig. 7). It can be seen from the figure that: (1) When the disturbing model is located to one side, the mean cross-wind coefficient of the disturbed model increases with decreasing lateral spacing ratio (the maximum value, 0.25, occurs at about (–1, 0.5)). In addition, the ridge of the contour is approximately located along the line $X/D = -1$. (2) When the disturbing model is far from the disturbed model in the upstream and downstream directions, the mean cross-wind coefficient tends to zero.

The distribution of AIF values calculated using the RMS cross-wind aerodynamic force for terrain C is shown in Fig. 8. It can be seen from this figure that: (1) When the disturbing model is located in a local area of the oblique upstream (i.e. $X/D = 3$–7, $Y/D = 1.5$–3.5), the AIF value mainly lies in the range between 1.0 and 1.3. This is because of the interaction between the shear layer of the perturbation model in the inclined upper reaches of the disturbed building and the disturbed building which leads to an increase in the sideways fluctuating value in the disturbed model. This result is consistent with the findings of Mara *et al.* (2014), however, their researches only focused on interference effects on a main building caused by an upstream disturbing building. (2) When the interfering building is located upstream, the AIF values are less than 1.0. This indicates that the RMS of the cross-wind aerodynamic force is reduced compared to the isolated building. It also gradually decreases with decreasing spacing ratio. (3) When the disturbing building is located to the side, the AIF value is less than 1.0 and increases as the spacing ratio increases laterally. When the separation between the two buildings reaches $3.5D$, the interference effect is very small.
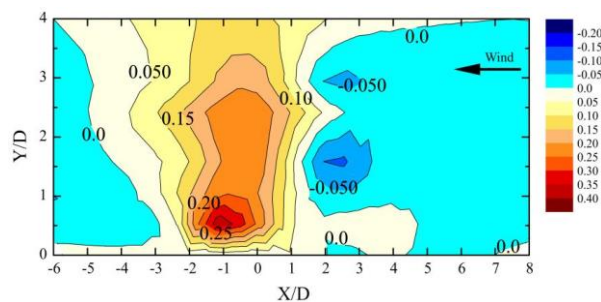

Fig. 7 Contour plot of the mean across-wind aerodynamic force coefficients for terrain C
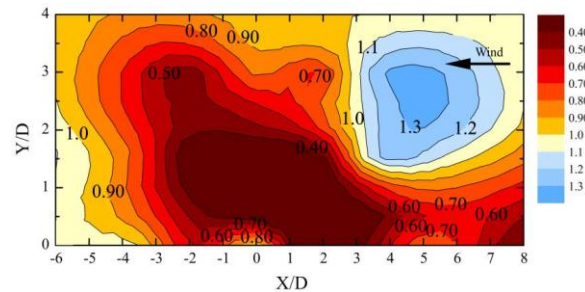
Fig. 8 AIF contour plot for the RMS across-wind aerodynamic force for terrain C

(4) When the building is located downstream, the AIF value is also less than 1.0, and gradually increases with an increase in the spacing ratio in the along-wind direction. Again, there is a valley in the interference contour at about 45°.

3.3 Torsional AIFs

As for the mean cross-wind aerodynamic coefficient, in the single state, the torsional aerodynamic coefficients for the disturbed model are theoretically equal to zero as the windward side of the model is perpendicular to the incoming flow and the surfaces are symmetrical. Thus, an analysis of the distribution of the AIF values for the cross-wind aerodynamic coefficient has little significance. Therefore, we only give here a contour map showing the mean torsional aerodynamic coefficients for the disturbed model in the interfered state themselves, as shown in Fig. 9. It can be seen that: (1) When the disturbing model is located to the side of the disturbed model, the mean values of the torsional aerodynamic coefficients are larger than zero, implying that counter-clockwise torques are generated. The maximum value, 0.75, which occurs at (0, 1.5), forms a peak in the contour map. This implies that the surface wind pressure on the disturbed model is asymmetric when the disturbing model is at its side, resulting in a larger torsional aerodynamic force. (2) When the disturbing model is located in an oblique upstream direction (0–45°), the mean values of the torsional aerodynamic coefficients are negative or zero, and a clockwise twist is produced. The map's minimum value of –0.60 occurs at (2, 0.5). Because of the semi-occluding effect of an oblique upstream disturbing model, the wind load on the disturbed model is asymmetrical. Thus, the mean value of the clockwise torsional aerodynamic coefficient of the disturbed model increases, and a ridge line (absolute value) appears in the contour at about 15°.

The RMS value of the torque reflects the asymmetric nature of the fluctuating wind load on the building. Fig. 10 shows a contour map of the distribution of the AIFs derived from the RMS torsional aerodynamic coefficient values for terrain C. The figure shows that: (1) When the disturbing model is located in the oblique upstream direction and near to the disturbed model (at about 5–60°), the AIF values are greater than 1.0 and reach a maximum value of 1.5. The ridge line of the contour is located at about 15°. Here, the fluctuating wind load on the disturbed model is not symmetrical, and the RMS value of the torsional aerodynamic coefficient is increased, especially when the disturbing model is located at (6.0, 1.0). This is because periodic vortex shedding occurs from the upstream disturbing model, and the complete vortex in the wake flow impacts non-symmetrically on the side of the disturbed model. (2) When the disturbing model is located right upstream and X/D is in the range 0.0 to 5.0, the AIFs are just slightly less than 1.0; when $X/D >$

5.0, they are essentially equal to 1.0. (3) When the disturbing model is located to one side and in the downstream, i.e., in the region (−2–2, 1–2), the AIF values are smaller than 1.0 and a basin is formed in the contour. When X/D approaches -4.0, the AIFs approach 1.0.

4. Wind pressure distributions and interference factors

The interference characteristics of the overall AIFs provide a macroscopic view of the interference. Such an approach is useful during the preliminary structural design stage, but cannot describe the interference properties (variation, degree, and mechanism involved) arising from the local wind load on the surface of the building. Therefore, based on the AIF distributions provided in Section 2, several typical operating arrangements (i.e. buildings in tandem, parallel, and staggered) were selected to analyze, in detail, the distribution of the local wind pressure coefficients on each surface and also the interference factors for the local wind pressure for several typical measurement layers.

4.1 Tandem arrangement

Two tandem arrangements, with the disturbing building upstream and downstream of the disturbed building, were selected for analysis. In the upstream case (i.e., the situation shown in Fig. 3), X/D was set equal to 1.5, 2.2, 3.5, 4.5, 5.5, and 7.5, that is, the disturbing building had coordinates (1.5,0), (2.2,0), (3.5,0), (4.5,0), (5.5,0), and (7.5,0), respectively. Similarly, for the downstream case, X/D was set equal to −1.5, −2, −3.5, and −5.5, i.e. the second building's coordinates were (−1.5,0), (−2,0), (−3.5,0), and (−5.5,0), respectively.
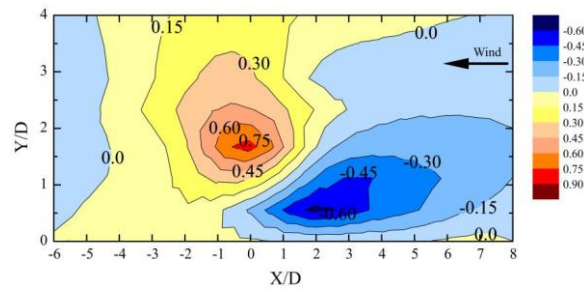

Fig. 9 Contour plot of the mean torsional moment coefficients for terrain C
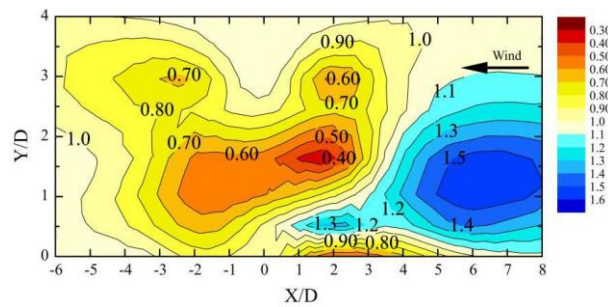

Fig. 10 AIF contour plot derived from the RMS values of the torsional moments for terrain C

4.1.1 Mean wind pressure coefficient distributions and interference factors I_f

To analyze the variety of the distributions of average wind pressure changed with the distance between disturbing and disturbed buildings and the interference degree, Figs. 11 and 12 give the cloud images of the distributions in the average wind pressure coefficients for each face of the model and the interference factors I_f on each key layer for different in-tandem (upstream) separation ratios, respectively. It can be seen from the figures that: (1) The average wind pressure coefficients on the middle and lower parts of the windward side (B) of the disturbed building (i.e., those lower than the height of the disturbing building) are significantly reduced and even become into negative pressure partly when the distance ratio (X/D) is less than 3.5. This is because the vortex street of the upstream disturbing model is suppressed, and subsequent high-speed separation shear flow is directly attached to the side of the disturbed model-this leads to the formation of a negative pressure zone in the middle and lower parts of the two models.
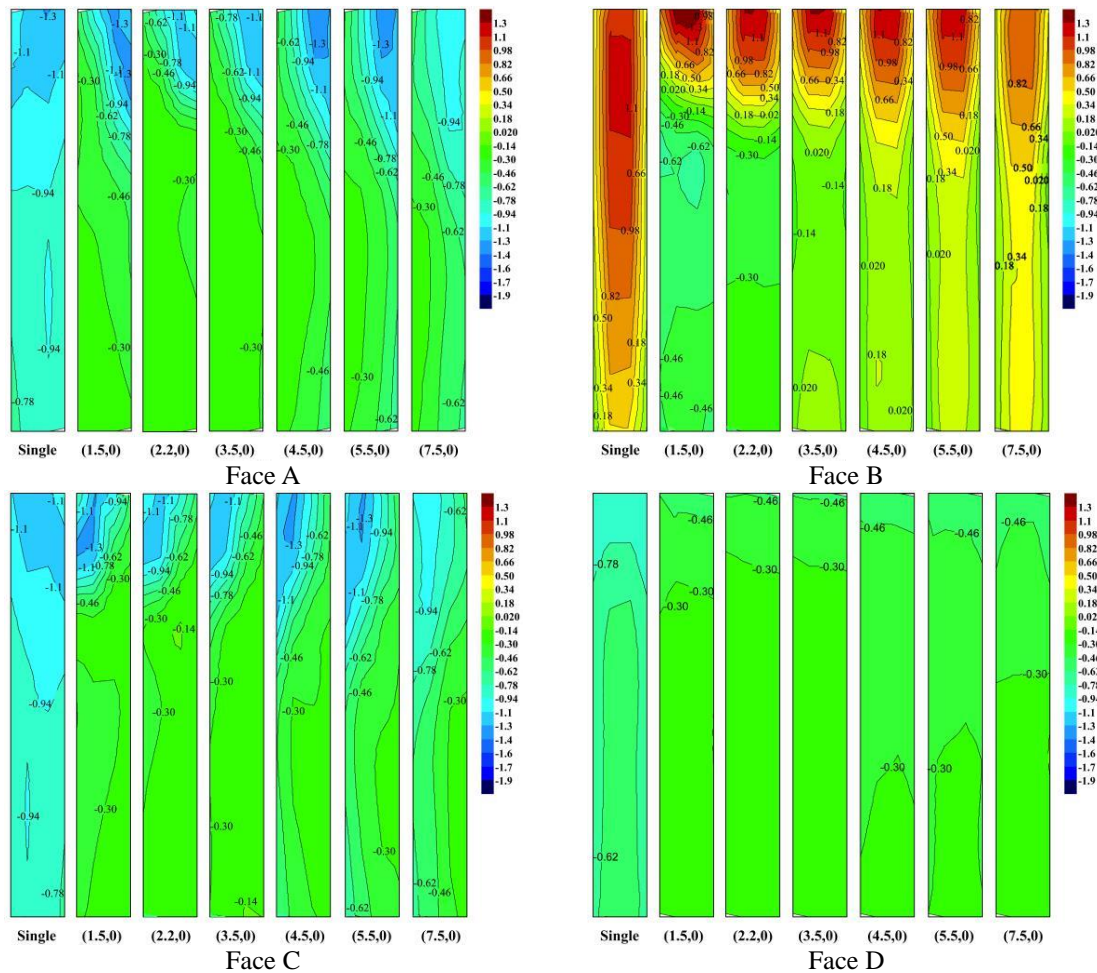

Fig. 11 Cloud images of the distributions of the average wind pressure coefficients for each face of the disturbed model and for different separation ratios (buildings in tandem-upstream)
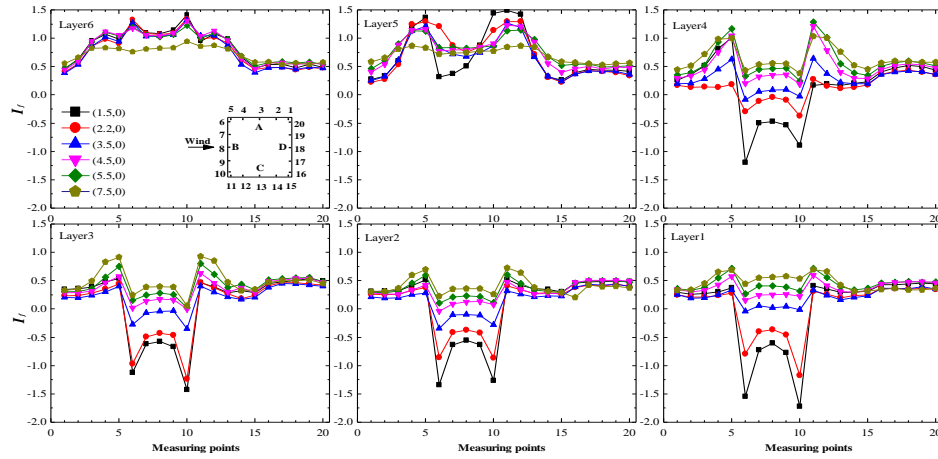
Fig. 12 Interference factors derived from the mean wind pressures on each measuring point and each layer for different distance ratios (buildings in tandem-upstream)

This clearly shows an obvious shielding effect and the interference is more obvious as the distance ratio decreases. The maximum absolute value of interference factors is equal to −1.75, appearing on the edge of the windward side. This explains why the mean values of the along-wind aerodynamic coefficients shown in Fig. 5 are less than 1.0 and decrease with decreasing distance ratio. When the distance ratio is small, the average wind pressure coefficients on the upper part of the windward side (B) of the disturbed building increase locally, the maximum interference factors can reach up to 1.5 at the two edges. This is because they are affected by the three-dimensional flow around the top of the disturbing building. (2) The variation in the average wind pressure coefficients on both sides (A and C) is basically symmetrical. In middle and lower parts, the wind pressure generally becomes smaller as the distance ratio decreases. This is because as the spacing ratio becomes smaller, the disturbed building lies further within the wake vortex street of the disturbing building and a wider negative-pressure zone forms between the two buildings. Thus, the separated flow on the leading edge of the side of the disturbed building is weakened, and suction on the side surface decreases. Compared to that on the trailing edge, the decrease in the suction is more obvious on the leading edge as the distance ratio decreases. However, on the upper part, the wind pressures are different, performance as increasing at the leading edge and decreasing at the trailing edge, the maximum interference factors can reach up to 1.5. (3) There is less interference on the leeward side compared to the other three surfaces. The absolute values of the negative pressures are about half smaller than those for an isolated building, and the change with distance is indistinctive.

Now consider when the disturbing building is located downstream in tandem. Fig. 13 shows the cloud images of the distributions in the average wind pressure coefficients for each face of the model for different in-tandem (downstream) separation ratios. It can be seen from the figures that, the average wind pressure coefficients on the windward (B) and leeward (D) sides change indistinctively as the distance changes. And that on the crosswind sides (A and C) become somewhat obvious if the spacing is small, Yahyai *et al*. (1992) found that when the spacing ratio between a downstream disturbing building and upstream disturbed building is about 2-3, the interference effects on the disturbed building are enhanced. Our findings coincide with their.
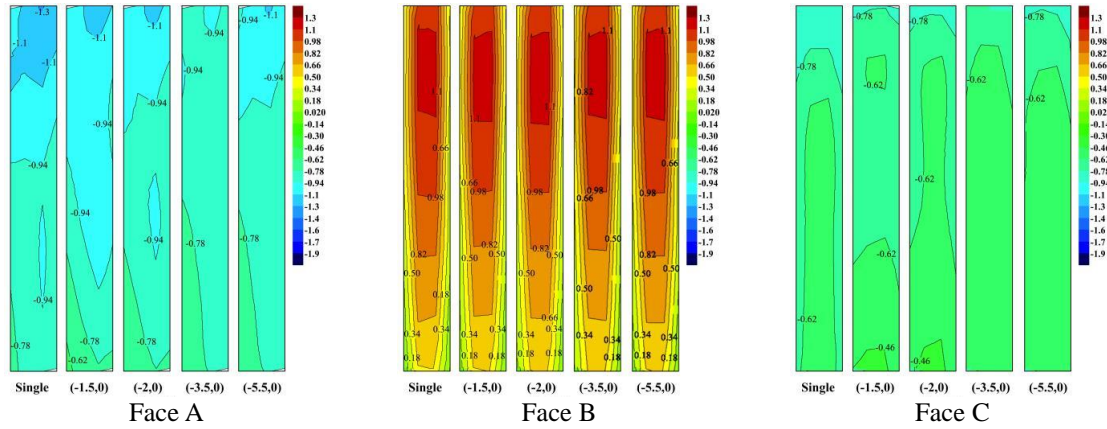
Fig. 13 Cloud images of the distributions of the average wind pressure coefficients for each face of the disturbed model and for different separation ratios (buildings in tandem- downstream)

4.1.2 Fluctuating wind pressure coefficients and interference factors I_f'

To analyze the variety of the distributions of fluctuating wind pressure changed with the distance between disturbing and disturbed buildings and the interference degree, Figs. 14 and 15 show the cloud images of the distributions in the fluctuating wind pressure coefficients for each face of the model and the interference factors I_f' on each key layer for different in-tandem (upstream) separation ratios, respectively.

It can be seen from Figs. 14 and 15 that when the disturbing model is located upstream: (1) The fluctuating wind pressure coefficients on the two edges of the windward side are significantly larger than those of the isolated building and gradually increase as the distance ratio decreases. This is especially so near the height of the disturbing model (e.g., layer 4), where the maximum interference factor (on the two edges) is close to 3.0. It is because that when the separation is relatively small, vortex shedding is suppressed and the signature turbulent flow is not fully dissipated in the relatively small space available. It then acts directly on the windward side of the downstream disturbed building, thereby significantly enhancing the turbulent fluctuations. (2) The fluctuating wind pressure coefficients on the leading edges of the side surfaces (A and C) are significantly different from those of the isolated building. When the spacing ratio is < 7.5, the affected area gradually increases as the distance ratio increases. When the spacing ratio is in the range 3.5 to 7.5, the interference factors on the sides exceed those found when the spacing ratio is less than 3.5. Also, those on the leading edges are basically larger than 1.0, the maximum interference factor (near the height of the disturbing model, e.g. layer 4) is close to 2.0, and those on the trailing edges are generally less than 1.0. This is because when the spacing ratio is in the range 3.5-7.5, periodic vortex shedding occurs after both the two models, and so the disturbed building is just located in the vortex zone of the upstream disturbing model. Vortex shedding directly impacts upon the edges of the side faces of the downstream (disturbed) model and makes the shear layer on the leading edge become rapidly separated, resulting in large fluctuations. However, when the two models are closer to each other, the wind pressure fluctuations on the side surfaces of the disturbed model are relatively weak as periodic vortex shedding cannot form behind the disturbing model. (3) The fluctuating wind pressure coefficients on the leeward side are smaller than those for an isolated building and decrease as the distance ratio decreases.
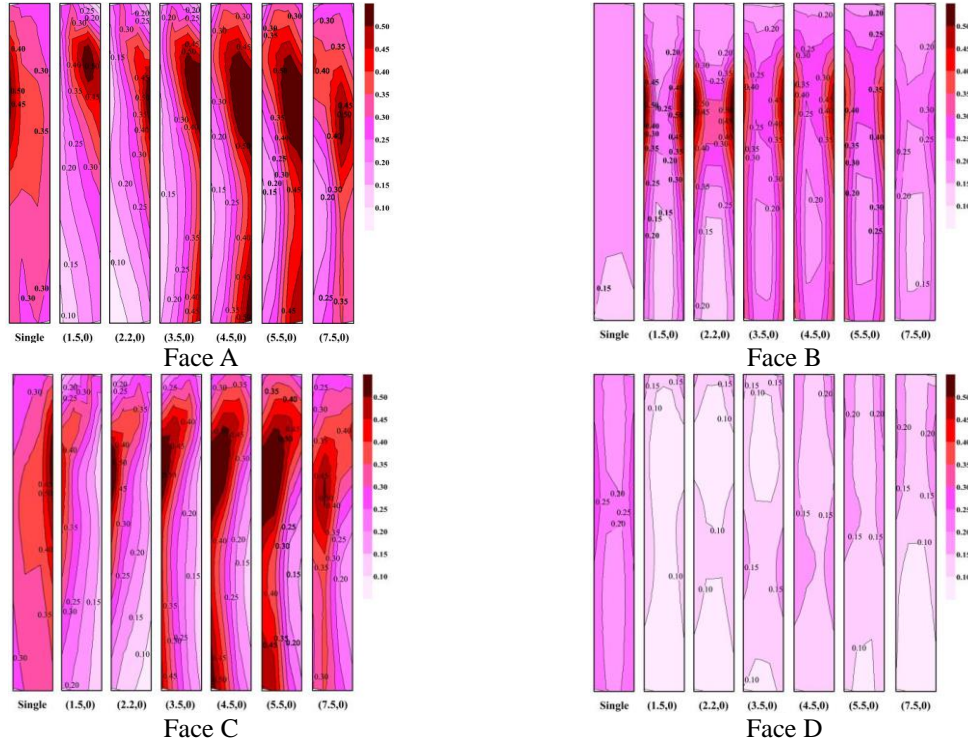
Fig. 14 Cloud images of the distribution of the fluctuating wind pressure coefficients on each face for different distance ratios (buildings in tandem-upstream)
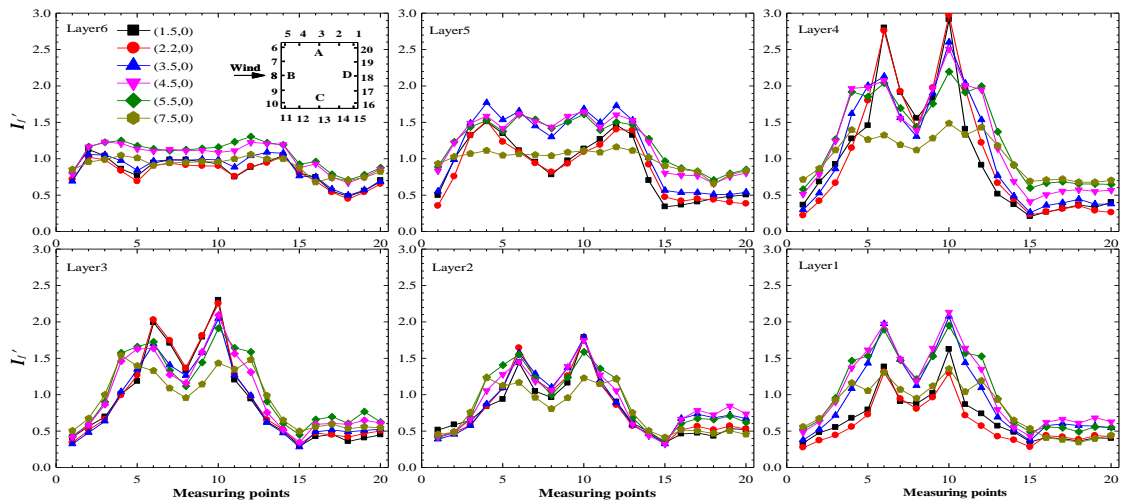

Fig. 15 Interference factors derived from the fluctuating wind pressures acting on each measuring point of each layer for different distance ratios (buildings in tandem-upstream)
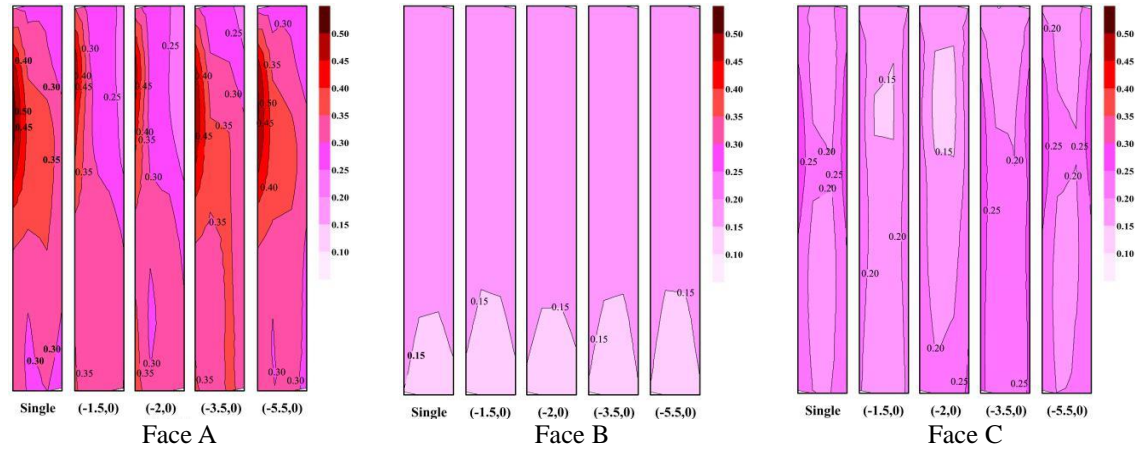
Fig. 16 Cloud images of the distribution of the fluctuating wind pressure coefficients on each face for different distance ratios (buildings in tandem-downstream)

Figs. 16 shows the cloud images of the distributions in the fluctuating wind pressure coefficients for each face of the model for different in-tandem (downstream) separation ratios. It can be seen that: (1) Regardless of distance, the fluctuating wind pressure coefficients on the windward side change little compared to those of an isolated building. (2) When the spacing ratio is less than –2.0 (absolute value comparison), the changes in the fluctuating wind pressure coefficients on the lateral trailing edges of upper part and the leeward side of the lower part are relatively large, that is due to the impact of the three-dimensional flow and ground friction on these layers. However, when the spacing ratio is larger than –3.5, the interference effect is negligible.

4.2 Side-by-side arrangement

Four typical situations were selected to investigate the side-by-side configuration, wherein *Y/D* is equal to 1.5, 2, 3, and 3.5, i.e., where the coordinates of the disturbing building are (0, 1.5), (0, 2), (0, 3), and (0, 3.5), respectively.

4.2.1 Mean wind pressure coefficients and interference factors I_f

Figs. 17 and 18 illustrate the distribution of the average wind pressure coefficients on each face and the interference factors I_f in each layer for different inter-building separations for the side-by-side arrangement, respectively. The figures show that in a side-by-side configuration: (1) The most obvious effects occur on side A (i.e., the slit side): the average negative pressures on side A (slit side) gradually become smaller from the leading edge to the trailing edge. And, as the distance ratio decreases, the leading edge interference factors become larger — the maximum value is close to 2.0 (Y/D = 1.5, layers 3 and 4), and the trailing edge interference factors become smaller — the minimum value is close to 0.4 (Y/D = 1.5, layers 3 and 4). Clearly, the smaller the spacing ratio, the greater the reduced amplitude of the interference factor from the leading to trailing edge, especially in the region lower and close to the height of the disturbing building. This is because the two square-sectioned models are constrained with a 'slit' between them.
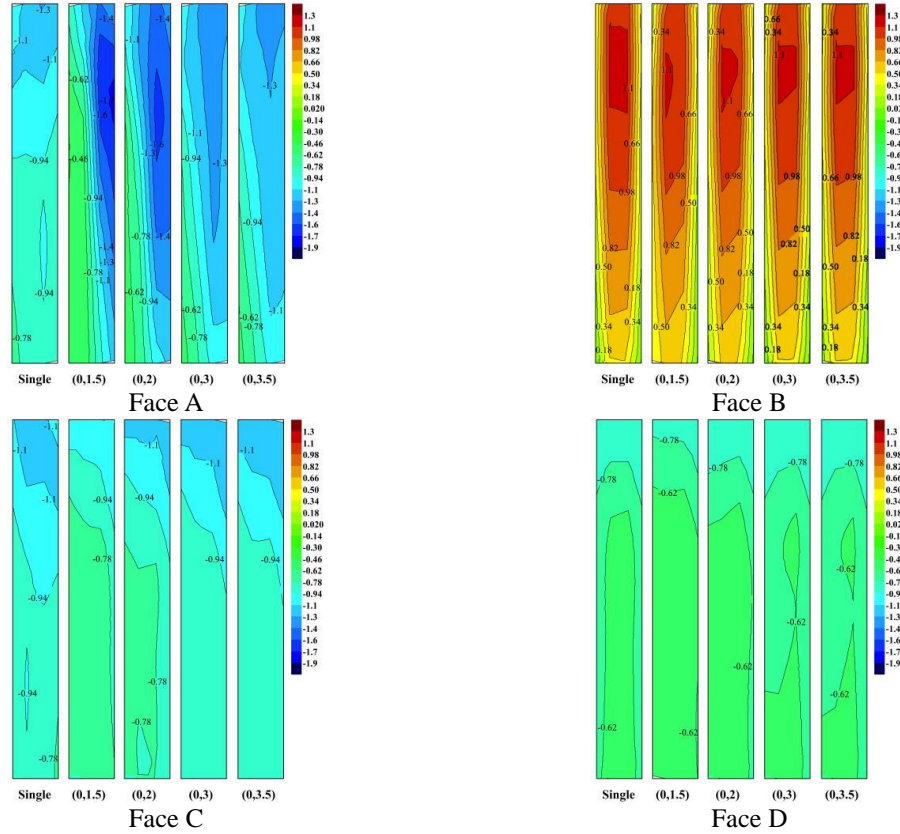
Fig. 17 Cloud images showing the distribution of the average wind pressure coefficients on each face for different separations between buildings (side-by-side configuration)

As the distance ratio decreases, the velocity of the airflow passing through the slit rapidly increases, resulting in a fast shear flow. Therefore, large negative pressures are generated on the side surface of the building, that is, there is a 'slit effect'. Subsequently, the airflow rapidly reduces due to the frictional resistance of the wall surface. (2) The average negative pressure coefficients on the leading edge of side C (the outer side) are slightly decreased when the distance ratio is less than 2.0, but the interference can be neglected when the spacing ratio is greater than 3.0. (3) Interference effects on the windward side (B) are not so obvious. However, the average wind pressure coefficients are slightly asymmetrical due to slit effects, and this asymmetry becomes more obvious as the distance ratio decreases-the interference factors on the edge near the inner side are increased, and those near the outer side are reduced, and the maximum value reached is 1.6. (4) When the spacing ratio is less than 2.0, the absolute value of the mean wind pressure coefficients on the lower part of the leeward side decreases. When the spacing ratio is more than 3.0, the mean wind pressure coefficients on the leeward side gradually approach those of the isolated building. This is consistent with the conclusions of the study by Chen *et al*. (2000), i.e., when the spacing ratio exceeds the critical value of 2.0, the fluid form of the building is changed (from partial flow to bistable flow), the two buildings both experience vortex shedding separately, and the aerodynamic characteristics of the leeward side tend to be stable.
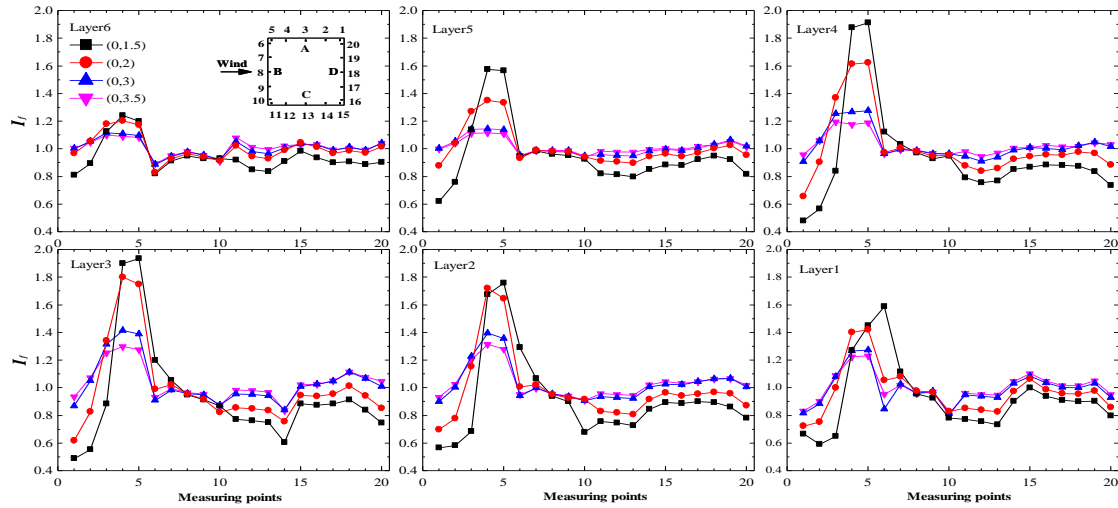
Fig. 18 Interference factors derived from the mean wind pressures acting on each measuring point in each layer for different separations between buildings (side-by-side configuration)

4.2.2 Fluctuating wind pressure coefficients and interference factors I_f'

Figs. 19 and 20 present the Cloud images of the average wind pressure coefficients on each face and the interference factors I_f' derived from the fluctuating wind pressures acting on the measurement points of each layer for different inter-building separations for the side-by-side arrangement, respectively. It can be seen from the figures that: (1) the interference effect found for side A (namely the slit surface) is the most prominent —as the spacing ratio decreases, the peak coefficient gradually shifts from the trailing to the leading edge, and the contour line becomes progressively steeper. The maximum interference factor is 1.4 and the minimum close to 0.3, and these are located at the front part and trailing edge, respectively. This is because a narrower slit has a stronger slit effect which leads to a stronger wind speed on the inner side. Then, the flow will more rapidly become separated at the leading edge of the buildings and the vortex shedding will become disordered. However, after passing the rear side it quickly tends to become uniform, so that the fluctuating wind pressure gradually decreases from front to back. When the spacing ratio exceeds 3.0, this phenomenon gradually disappears. (2) As the distance ratio decreases, the fluctuating wind pressure coefficients on side C (the outer side) gradually decrease, and most of the interference factors are between 0.5 to 1.0. (3) Due to the more direct influence of the incoming flow, the interference factors on the windward side mostly are less affected by the spacing ratio except some points near to the edge of the slit, the interference factors at which decrease something as the distance ratio decreases. (4) As the distance ratio decreases, the fluctuating wind pressure coefficients on the leeward side of the disturbed model are smaller than those of an isolated building, and the interference factors increase gradually from 1.0 to about 0.5 as the distance ratio decrease. When the spacing ratio larger than 3.0, the interference factors tend to be more stable and less influenced by separation.
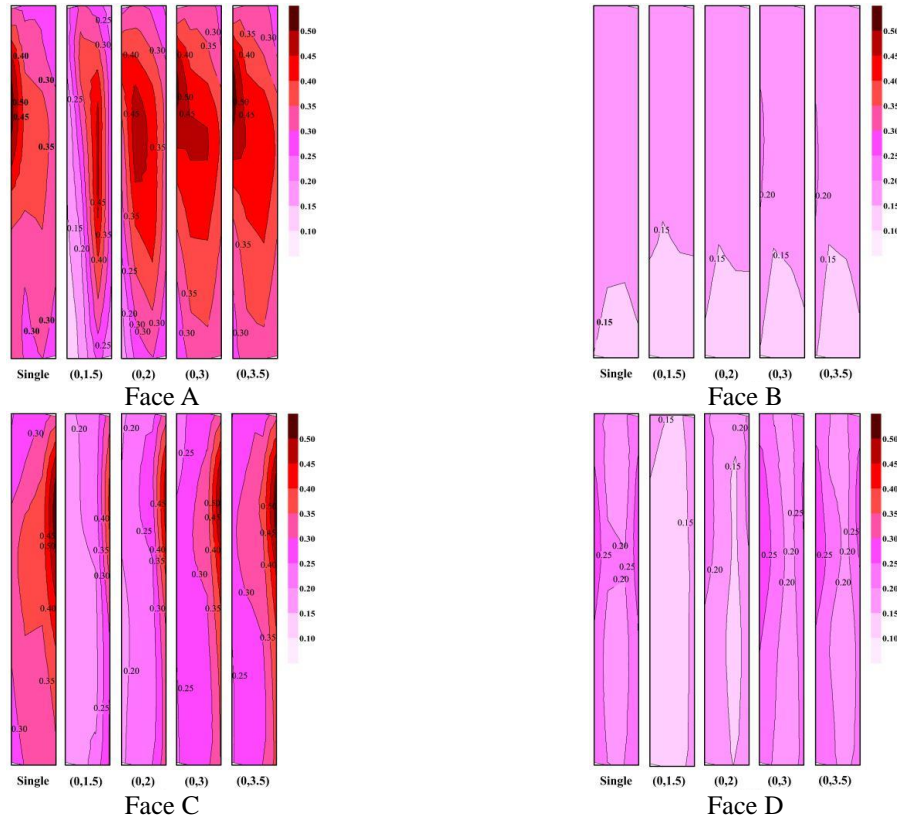
Fig. 19 Cloud images showing the distribution of the fluctuating wind pressure coefficients on each face for different separations between buildings (side-by-side configuration)
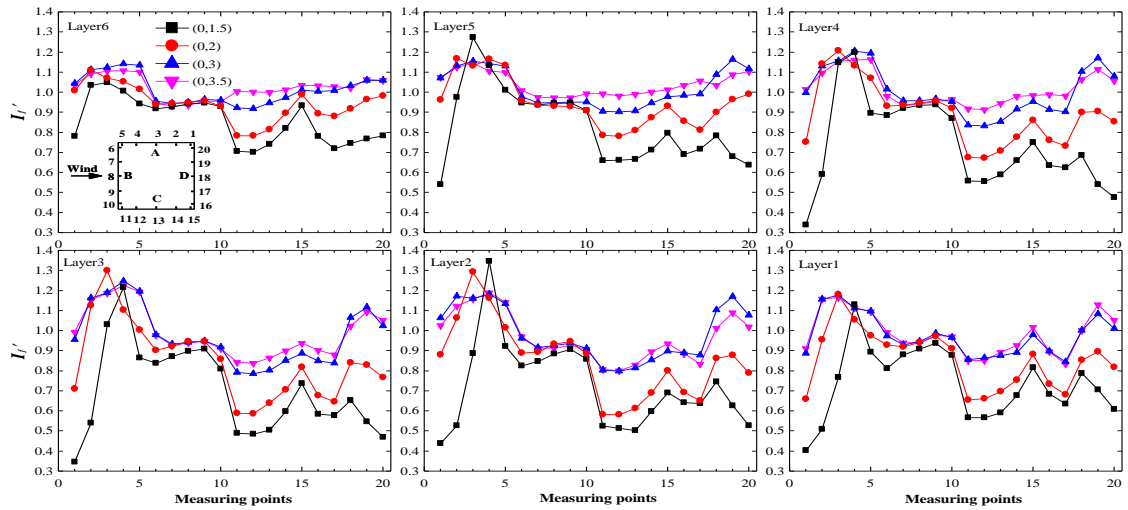

Fig. 20 Interference factors derived from the fluctuating wind pressures on each measuring point in each layer for different separations between buildings (side-by-side configuration)

4.3 Staggered arrangement

Four typical conditions were selected to investigate the use of a staggered configuration corresponding to setting *X/D* to 1.5, 2, 3.5, and 5.5, and *Y/D* to 1.5. That is, the disturbing building is placed at the locations with coordinates (1.5, 0.5), (2, 0.5), (3, 0.5), and (3.5, 0.5), respectively. In this section, the term 'distance ratio' refers just to the *X/D* ratio.

4.3.1 Mean wind pressure coefficients and interference factors I_f

Figs. 21 and 22 give the cloud image distributions of the average wind pressure coefficients on each face and the interference factors derived from the average wind pressures acting on the measurement points of each layer for different distance ratios in the staggered configuration, respectively. The figures show that: (1) The interference on the windward side (B) is significant and asymmetric. Part of the wind load acting on the windward side is influenced by shielding and the other by the high speed separation shear flow of the upstream disturbing model. More the separation decreases, more the asymmetry is. Therefore, the maximum positive interference factor appears on the unshielded part of the windward side when the distance ratio is smallest, which is close to 1.6, and the largest negative interference factor appears on the shielded part of the windward side and its value is close to −1.2. (2) The changes on lateral side C (the outer side) are also remarkable. The pressure on the leading edge part is amplified, and the maximum interference factor found is close to 1.6. However, the pressure on the trailing edge appears to be diminished, with a minimum interference factor close to zero. (3) The average wind pressures on the side A (the sheltered side) and the leeward side (D) are smaller than that of an isolated building, and the interference factors mainly concentrated in the range 0.4–0.8. (4) The top of building is hardly affected by the spacing ratio. Only part of the windward side (near to side C) has factors that are greater than 1.0, and the maximum valued reached is 1.4.

4.3.2 Fluctuating wind pressure coefficients and interference factors I_f'

Figs. 23 and 24 show cloud images of the distribution of the fluctuating wind pressure coefficients on each face and the interference factors derived from the fluctuating wind pressures acting on each of the measurement points for different distance ratios in the staggered configuration, respectively. It can be seen from the figures that: (1) The fluctuating wind pressure coefficients on the middle and lower parts of the windward side are not symmetrical due to the complex interaction between the incoming flow and the wake and shear layer of the disturbing model, also, the smaller the separation, the stronger the asymmetry. As the separation decreases, it leads to an amplification effect on the unsheltered part -affected by the shear layer of the disturbing model (with a maximum interference factor of 3.5, happening in the middle and higher part of the model), and a reduction effect on the other-sheltered part (with a minimum interference factor close to 0.75). (2) The fluctuating wind pressure coefficients on side A (the sheltered lateral side) are clearly distributed very differently to those obtained using an isolated building. More specifically, the peak coefficient on the side A shifts from being on the trailing edge in the isolated building to the leading edge in the disturbed state. Furthermore, as the distance ratio increases, the fluctuating pressure coefficients and the area over which the peak values are distributed on the side A gradually increase. It is worth noting that, as the separation increases, the interference factor of the fluctuating wind pressure on the side A (including the edge at shielded windward side) gradually increases to such an extent that (when the spacing ratio > 2) it basically becomes an amplification effect (with a maximum value close to 2.0 when the spacing ratio equals to 5.5). This

is because the disturbed model is closer to the wake edge of the disturbing model when the spacing is relatively large, so that the fluctuating interference is enhanced. However, when the spacing is relatively small, regular vortex shedding cannot form behind the disturbing model. (3) The interference characteristics of fluctuating wind pressures on side C (the unsheltered lateral side) are somewhat similar to side A: the peak coefficient shifts from being on the trailing edge in the isolated building to the leading edge in the disturbed state as the disturbing building is constantly approaching the target building, and the zone of wind pressure amplification is gradually decreases. It is to say, as the distance ratio decreases, the area which interference factors larger than 1.0 at the leading edge decreases — the maximum interference factor is close to 2.0 (at middle upper part), and the area which interference factors less than 1.0 at the trailing edge increases — the minimum interference factor is less than 0.25. (4) The fluctuating wind pressure coefficients on the leeward side are smaller than those of the isolated building for the disturbing model changing the wake pattern of the disturbed model. Furthermore, the interference factors get lower as the separation decreases. (5) The fluctuating wind pressures on the windward side and the lateral sides of the upper part of the building are basically larger than isolated one and increase as the distance ratio increases. The maximum interference factor exceeds 1.5.
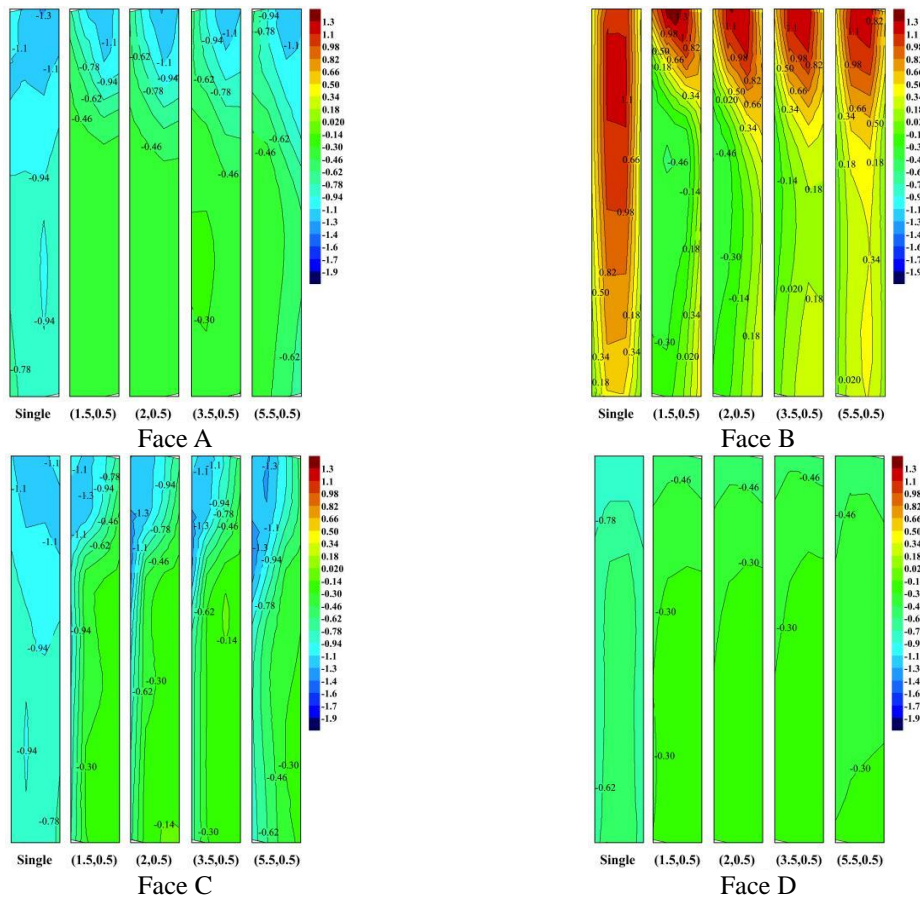

Fig. 21 Cloud images showing the distribution of the average wind pressure coefficients on each face for different separations between buildings (staggered configuration)
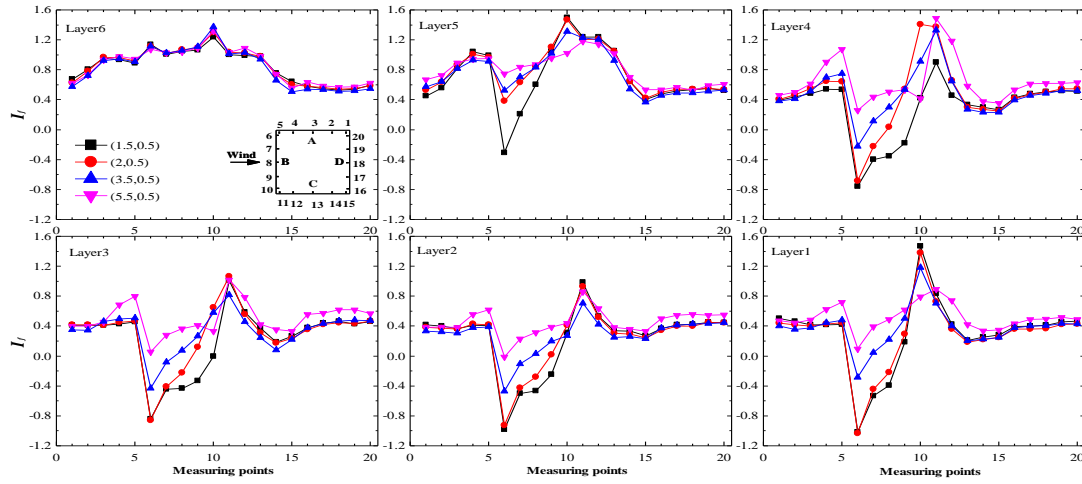
Fig. 22 Interference factors derived from the mean wind pressures on each measuring point in each layer for different distances between buildings (staggered configuration)
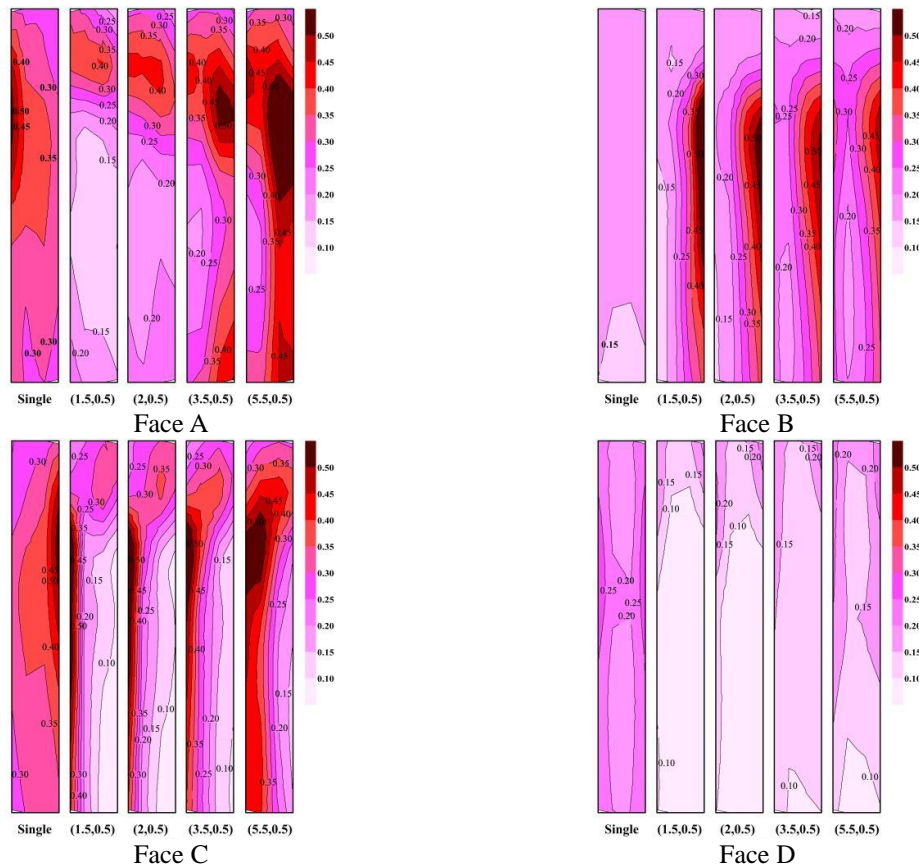

Fig. 23 Cloud images showing the distribution of the fluctuating wind pressure coefficients on each face for different separations between buildings (staggered configuration)
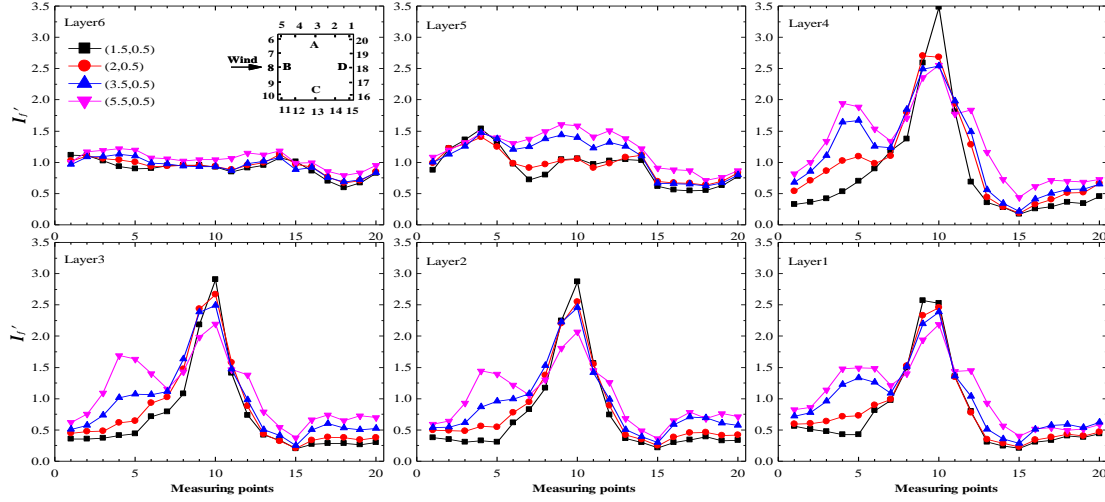
Fig. 24 Interference factors derived from the fluctuating wind pressures on each measuring point in each layer for different distances between buildings (staggered configuration)

5. Energy spectra results and analysis

The contribution of the incoming turbulent flow and the signature turbulence of the fluid–structure interaction to the fluctuating energy of the wind pressure acting on a building's surface are reflected in the spectra of them. For high-rise buildings, it is useful to analyze the fluctuating aerodynamic spectra for each layer. To date, much research has been carried out on the fluctuating wind spectra of isolated high-rise buildings. However, little research has been carried on the aerodynamic spectral characteristics of interfered high-rise buildings. The strength of the periodic vortex shedding is reflected by the main peak in the fluctuating lift force spectrum. In addition, the frequency of the vortex shedding corresponds to the frequency of the peak in the spectrum. Hence, in this section, we analyze the interference characteristics of the wind loads acting on the tall buildings in the frequency domain in the form of fluctuating lift force spectra.

The across-wind fluctuating aerodynamic spectra given below are all normalized power spectra. On their ordinates we plot $nS(n)/\sigma^2$, where $S(n)$ is fluctuating aerodynamic spectrum, n is the fluctuating aerodynamic frequency, and σ^2 is fluctuating aerodynamic variance. Their abscissae correspond to the dimensionless reduced frequency nB/U, where B is the width of the windward side of the building and U is the average wind speed at the top of the building. In this work, we use f^* to represent the reduced frequency.

Fig. 25 shows the across-wind lift fluctuating spectra for the different layers of an isolated building. As can be seen from the figure, due to vortex shedding, the spectrum of each layer has a significant narrowband peak. The peak is produced by flow separation, transient reattachment, and the vortex effect. Although the vortex shedding intensities at the different heights are different, the vortex shedding frequency is consistent among each layer. The reduced frequency corresponding to the peak in the spectrum is 0.101 (referred to as its Strouhal number). This is slightly smaller than the Strouhal numbers for two-dimensional square cylinders, i.e., 0.125–0.13. The interference

effects between the disturbing and disturbed buildings will be separately discussed for each of three configurations considered in turn (in-tandem, side-by-side, and staggered).

5.1 In-tandem arrangement

It has been found that an upstream (interfering) building can increase the broadband disturbance to the flow around a downstream (interfered) building, thereby reducing its across-wind response and, in addition, the vortex shedding peak (Lam *et al.* 2008). Therefore, it is necessary to analyze the across-wind fluctuating lift spectrum of each layer of the building in detail.

Fig. 25 also shows the across-wind fluctuating lift force spectra of each layer under different conditions in the upstream in-tandem configuration. Comparing the spectra with those from the isolated building, we can see that when the perturbing model is located in the upstream: (1) The shapes of the across-wind fluctuating lift force spectra for each layer are roughly the same for the different spacing ratios. They all have peaks, but the peaks are reduced in height compared to the isolated building: the peaks in the upper parts being reduced more than those of the lower parts. This indicates that the upstream building reduces the strength of the vortex shedding and that the effect on the upper part of the building is most apparent (due to the influence of three-dimensional turbulent flow there). (2) When the along-wind spacing ratio is less than 3.5, the bandwidth of the lift force spectra broaden markedly in each layer, and there is no pronounced narrowband peak (making the peak frequency difficult to determine). This is because, when the distance between the two models is small, the shear layer generated by the separation flow of the upstream model on both sides inhibits the periodic vortex shedding of the downstream (disturbed) model. This causes the spectral peak to disappear and the high frequency energies (i.e., $0.7 \leq f^* \leq 1.0$) to increase significantly. When the spacing ratio is greater than 3.5, this phenomenon only appears in the upper part of the model. This is because the periodic vortex shedding formed by the upstream model does not affect the vortex shedding of the downstream disturbed model when the spacing ratio increases by a certain amount. However, the complex effects due to the three-dimensional turbulent flow at the top of the disturbing model are still present.
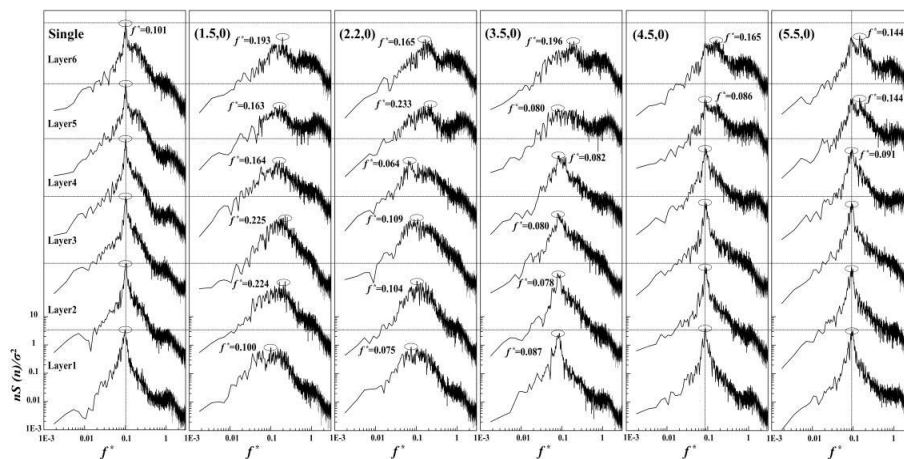

Fig. 25 Across-wind fluctuating lift force spectra for each layer under different conditions (in-tandem upstream configuration)
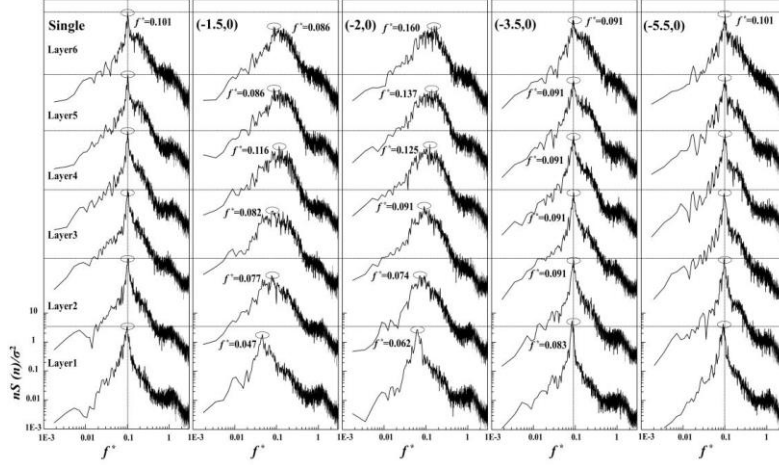
Fig. 26 Across-wind fluctuating lift force spectra for each layer under different conditions (in-tandem downstream configuration)

Fig. 26 presents the equivalent spectra to those in Fig. 25 for the downstream in-tandem configuration. The spectra show that when the perturbing model is located in the downstream: (1) The shapes of the across-wind fluctuating lift force spectra for each layer are essentially the same for different spacing ratios. They all have peaks in their spectra but the peaks are again reduced compared to the isolated building. This shows that the vortex shedding intensity in each layer is again reduced (and that the amplitude reduces more as the distance ratio decreases). (2) When the disturbing model is downstream, the interference in the across-wind fluctuation lift spectra of the disturbed model is only obvious when the separation is small (e.g., $X/D = -1.5$, 2.0). This is because the wake vortex street of the perturbative model is suppressed at this time (and the higher up, the more obvious this becomes) and the high-speed separated shear layer is directly attached to the downstream model's side. When the spacing ratio is greater than -3.5 (absolute value), the spectral peaks become more obvious (except for the upper part of the model), and their amplitude reduction is smaller.

5.2 Side-by-side arrangement

Fig. 27 shows the spectra produced when the buildings are side-by-side. For this configuration: (1) The shapes of the spectra for each layer are basically the same for the different spacing ratios, and they all have peaks. When the spacing ratio is less than 3.0, the spectral peaks are reduced in height compared to the isolated building's. This shows that the vortex shedding intensity at each height is reduced (as the distance ratio decreases, the amplitude becomes smaller, as before). (2) When the spacing ratio is 1.5, the bandwidths of the peaks in each layer's spectra are significantly widened, and a distinct narrowband peak does not appear in the upper layers' spectra (so the peak frequency is difficult to determine). Moreover, the energy of the high-frequency region (with reduced frequencies ~1.1) is significantly increased. This is because the wind speed through the slit is great, the magnitude of the vortex shedding is reduced, and the number of small-sized vortex shedding events is significantly increased compared to the isolated building case. When the

across-wind spacing ratio is greater than 2.0, the spectrum for each layer shows an obvious peak with narrow bandwidth. As the spacing ratio increases, the vortex shedding frequency in each layer approaches the same value. At the same time, the fluid form behind the models is transferred from the partial state into bistable flow, and the vortex shedding occurring from the two models occurs independently. (3) When the across-wind spacing ratio is less than 3.0, the vortex shedding frequency tends to increase as the spacing ratio increases, and the energy also gradually increases. When the across-wind spacing ratio is greater than 3.0, the vortex shedding frequency begins to decrease but the energy continues to increase. Eventually the vortex frequency and energy approaches that of the isolated building, and the interference disappears.

5.3 Staggered arrangement

Fig. 28 shows the spectra produced using the staggered configurations. For this position: (1) The shapes of the spectra are basically the same for the different spacing ratios. There are peaks, and they are reduced in height compared to the isolated building's, indicating that the interfering model decreases the strength of the vortex shedding. (2) When spacing ratio is less than 3.5, the bandwidth of the band in each layer becomes significantly wider. Again, there are no clear and consistent narrow peaks and therefore the peak frequency is difficult to determine. This is because, when the along-wind distance is small, the shear layer generated by the separation flow of the upstream disturbing model on both sides inhibits the periodic vortex shedding of the downstream disturbed model. This makes the peaks in the spectra disappear, the frequency of spectrum of each layer becomes inconsistent, and the energy of the high-frequency part of the spectrum is significantly increased. When the spacing ratio is greater than 3.5, this phenomenon only appears in the upper part of the disturbed building. The vortex shedding frequencies of the lower parts converge and are slightly smaller than those of the isolated building.
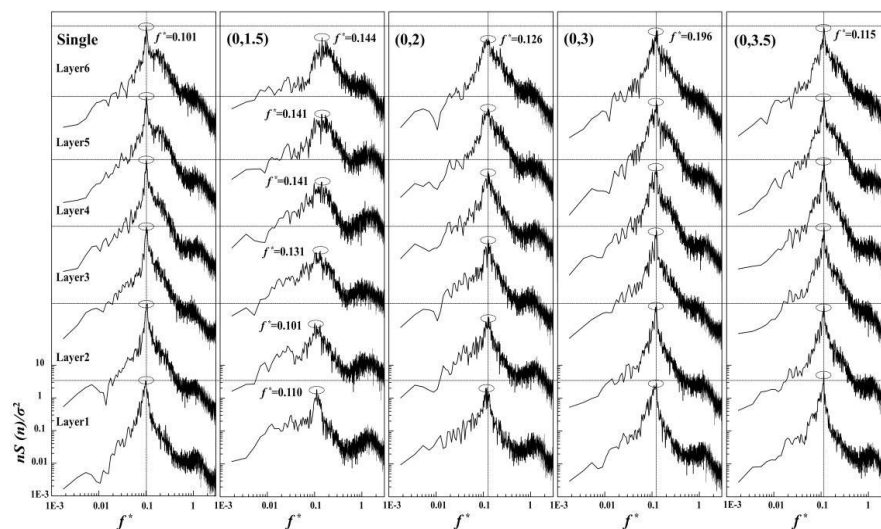

Fig. 27 Across-wind fluctuating lift force spectra for each layer under different conditions (side-by-side configuration)
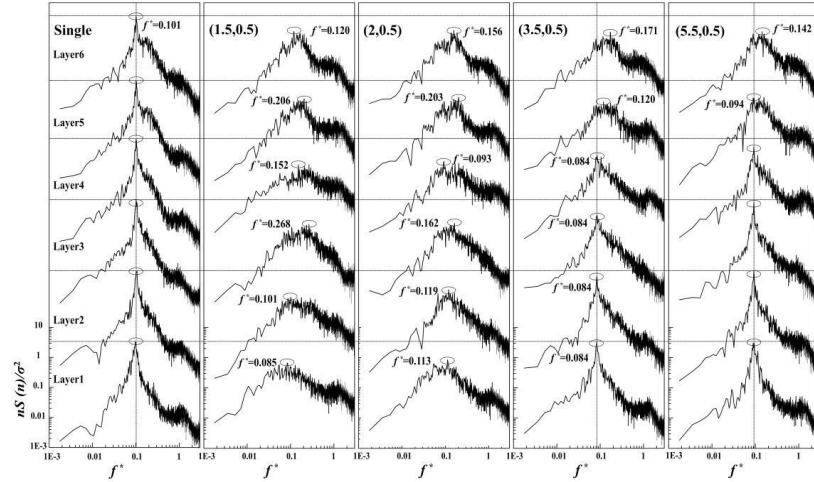
Fig. 28 Across-wind fluctuating lift force spectra for each layer under different conditions (staggered configuration)

6. Conclusions

In this paper, we have examined the interference effects arising due to the wind load acting on two identically-square cross-sectioned high-rise buildings of different height in detail via wind tunnel experiments on rigid models placed in different relative positions. Some important conclusions can be drawn, as follows:

(1)   When the interfering building is located directly upstream, the overall mean along-wind aerodynamic force on the disturbed building decreases significantly due to a sheltering effect. When the same interfering building is offset somewhat (i.e., is in an oblique upstream position), the mean torsional aerodynamic force on the disturbed building increases. The combined effect of the superimposed wake from the upstream building and incoming flow creates a large increscent adverse interference effect on the along-wind, across-wind, and torsional fluctuating aerodynamic forces when in the range of $X/D = 5$–6 and $Y/D = 0.5$–2.

When the disturbing building is located to the side of the disturbed building and the spacing between the models is small (e.g., Y/D is between 0 to 2), significant slit effects may arise. As a result, the interference factors in the mean along-wind aerodynamic force, and the along-wind, across-wind, and torsional fluctuating aerodynamic forces decrease, however, the across-wind and torsional mean aerodynamic forces may increase.

When the disturbing building is located directly downstream, the aerodynamic interference on the disturbed building is not obvious. That in an oblique upstream position has a slight impact.

(2)   When the interfering building is located in the right upstream, the mean wind pressure acting on the sheltered windward side of the disturbed building experiences significantly adverse interference: The ordinarily positive pressure will become negative and the interference effect has a maximum absolute value up to **1.75** times when the spacing ratio decreases to 1.5. Moreover, the fluctuating wind pressure on the sheltered windward side and leading edges of the sides increases significantly as the spacing ratio decreases, up to a maximum of 3.0 times.

When the interfering building is located to one side, the mean and fluctuating wind pressures on the leading edge of the side of the disturbed building (i.e., the inner lateral side) increase significantly as the spacing ratio decreases, up to a maximum of 2.0 times and 1.4 times, respectively.

When the interfering building is in a staggered upstream position (i.e., the disturbed building is only half-shielded by the upstream building), the average and fluctuating wind pressures on the non-sheltered edge of the windward side and leading edge of the side increase to a certain extent if the distance is small, maximum effect up to 1.5 times and 3.5 times, respectively. However, the fluctuating wind pressure on the sheltered part of the windward side decreases as the spacing ratio decreases within the range 1.5 to 5.5, and becomes larger than that of an isolated building for spacing ratios in the range from 3.5 to 5.5 (up to a maximum of **2** times).

When the disturbing building is located in the downstream, the changes in the average and fluctuating wind pressures acting on the disturbed building's surfaces are not obvious.

Moreover, for the effect of the three-dimensional flow around the top of the disturbing building, the average and fluctuating wind pressures on upper part of the windward side and side faces of the disturbed building experience adverse interference effects as the spacing ratio decreases, they would be up to a maximum of **1.5** times and **2** times, respectively.

(3)   When the interfering building is located upstream, the broadband disturbance due to the incoming flow acting on the downstream disturbed building increases. This reduces the peak heights in the fluctuating lift spectra (i.e. decreases the vortex shedding intensity), and the high-frequency energies increase significantly. When the spacing ratio is ≤3.5, the vortex shedding has no fixed periodicity, and the value of the peak frequency is difficult to determine. As the spacing ratio increases, the impact of the interference gradually weakens and disappears.

When the interfering building is located downstream, the interference in the across-wind fluctuating lift spectra is obvious only if the spacing ratio less than 2.0.

When the disturbing building is located to one side, slit effects causes the wind speed to increase significantly when the spacing ratio is less than 2.0 whereupon the vortex shedding intensity is reduced. The number of small-scale vortex events increases significantly compared to the isolated building, the spectral band broadens markedly, and there is no pronounced narrowband peak. As the spacing ratio increases, this phenomenon gradually disappears.

Acknowledgments

References

American Society of Civil Engineers (ASCE) (2010), *Minimum design loads for buildings and other structures*[S], ASCE/SEI. ASCE, New York, USA.

Blazik, B.E. (2006), "Interference loads of two cylinders in a side-by-side arrangement", *Wind Struct.*, **9**(1), 75-93.

Chen, S.Q., Gu, M. and Huang, Z.P. (2000), "Numerical computation of the flow around two square cylinders arranged side by side", *J. Appl. Math. Mech.*, **21**, 131-146. (in Chinese).

GB 50009-2012 (2012), *Load code for the design of building structures*. Ministry of Construction P.R. China, Beijing (in Chinese).

English, E.C. (1990), "Shielding factors from wind-tunnel studies of prismatic structures", *J. Wind Eng. Ind. Aerod.*, **36**, 611-619.

Huang, P. and Gu, M. (2005), "Experimental study on wind-induced dynamic interference effects between two tall buildings", *Wind Struct.*, **8**(3), 147-161.

Huang, D.M., Zhu, L.D., Chen, W. and Ding, Q.S. (2015), "Vertical coherence functions of wind forces and influences on wind-induced responses of a high-rise building with section varying along height", *Wind Struct.*, **21**(2), 119-158.

Hui, Y., Tamura, Y. and Yoshida, A.(2012), "Mutual interference effects between two high- rise building models with different shapes on local peak pressure coefficients", *J. Wind Eng. Ind. Aerod.*, **104-106**, 98-108.

Hui, Y., Yoshida, A. and Tamura, Y. (2013), "Interference effects between two rectangular-section high-rise buildings on local peak pressure coefficients", *J. Fluids Struct.*, **37**, 120-133.

Ke, S.T., Liang, J., Zhao, L. and Ge, Y.J. (2015), "Influence of ventilation rate on the aerodynamic interference between two extra-large indirect dry cooling towers by CFD", *Wind Struct.*, **20**(3), 449-468.

Khanduri, A.C., Stathopoulos, T. and Bedard, C. (1998), "Wind-induced interference effects on buildings-A review of the state-of-the-art", *J. Eng. Struct.*, **20**(7), 617-630.

Lam, K.M., Leung, M.Y.H. and Zhao, J.G. (2008), "Interference effects on wind loading of a row of closely spaced tall buildings", *J. Wind Eng. Ind. Aerod.*, **96**, 562-583.

Lim, J. and Bienkiewicz, B. (2014), "Wind tunnel investigation of correlation and coherence of wind loading on generic tall twin buildings in close proximity", *Wind Struct.*, **18**(4), 443-461.

Mara, T.G., Terry, B.K., Ho, T.C.E. and Isyumov, N. (2014), "Aerodynamic and peak response interference factors for an upstream square building of identical height", *J. Wind Eng. Ind. Aerod.*, **133**, 200-210.

National Research Council of Canada (NRCC) (2010), *National Building Code of Canada (NBCC)*, Institute for Research in Construction, Ottawa, ON.

Sakamoto, S. and Haniu, H. (1988), "Aerodynamic forces acting on two square prisms placed vertically in a turbulent boundary layer", *J. Wind Eng. Ind. Aerod.*, **31**(1), 41-66.

Taniike, Y. (1992), "Interference mechanism for enhanced wind forces on neighboring tall buildings", *J. Wind Eng. Ind. Aerod.*, **42**(1-3), 1073-1083.

Thepmongkorn, S., Wood, G.S. and Kwok, K.C.S. (2002), "Interference effects on wind-induced coupled motion of a tall building", *J. Wind Eng. Ind. Aerod.*, **90**, 1807-1815.

Wang, F., Tamura, Y. and Akihito, Y. (2014), "Interference effects of a neighboring building on wind loads on scaffolding", *J. Wind. Eng. Ind. Aerod.*, **125**, 1-12.

Xie, Z.N. and Gu, M. (2004), "Mean interference effects among tall buildings", *Eng. Struct.*, **26**, 1173-1183.

Xie, Z.N. and Gu, M. (2005), "A correlation-based analysis on wind-induced interference effects between two tall buildings", *Wind Struct.*, **8**, 163-178.

Yahyai, M., Kumar, K., Krishna, P. and Pande, P.K. (1992), "Aerodynamic interference in tall rectangular buildings", *J. Wind Eng. Ind. Aerod.*, **41**, 859-866.

Zhao, J.G . and Lam, K.M. (2008), "Interference effects in a group of tall buildings closely arranged in an L- or T-shaped pattern", *Wind Struct.*, **11**(1), 1-18.

CC